ACS APPLIED MATERIALS & INTERFACES

Research Article

www.acsami.org

Low-Temperature Metal-Oxide Thin-Film Transistors Formed by Directly Photopatternable and Combustible Solution Synthesis

You Seung Rim, Hyun Soo Lim, and Hyun Jae Kim*

School of Electrical and Electronic Engineering, 50 Yonsei-ro, Seodaemun-gu, Yonsei University, Seoul 120-749, Korea

Supporting Information

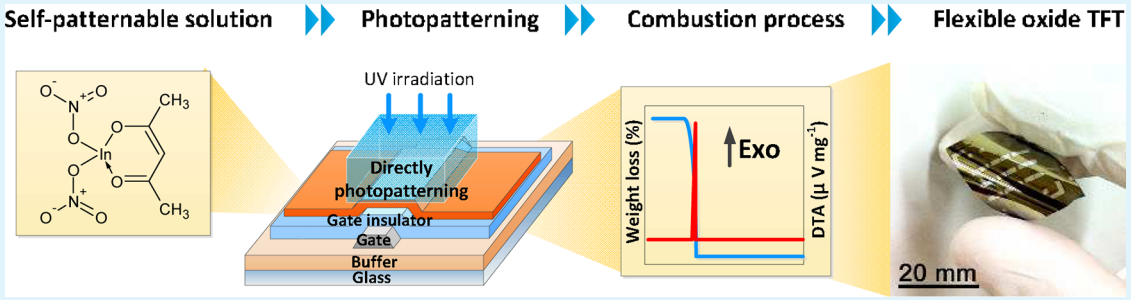

ABSTRACT: We investigated the formation of ultraviolet (UV)-assisted directly patternable solution-processed oxide semiconductor films and successfully fabricated thin-film transistors (TFTs) based on these films. An InGaZnO (IGZO) solution that was modified chemically with benzoylacetone (BzAc), whose chelate rings decomposed via a $\pi-\pi^*$ transition as result of UV irradiation, was used for the direct patterning. A TFT was fabricated using the directly patterned IGZO film, and it had better electrical characteristics than those of conventional photoresist (PR)-patterned TFTs. In addition, the nitric acid (HNO_3) and acetylacetone (AcAc) modified In_2O_3 (NAc-In_2O_3) solution exhibited both strong UV absorption and high exothermic reaction. This method not only resulted in the formation of a low-energy path because of the combustion of the chemically modified metal-oxide solution but also allowed for photoreaction-induced direct patterning at low temperatures.

KEYWORDS: *solution process, metal oxide semiconductor, photo patterning, low-temperature synthesis, flexible electronics*

1. INTRODUCTION

Solution-processed inorganic materials and the processes associated with them have attracted much attention for use in optoelectronics and display backplane technologies because of their advantages, such as the ability to print selectively, use roll-to-roll technologies, and control the atomic composition of the formed films easily. These processes are also advantageous because they involve simple processing steps.[1−4] Furthermore, a solution process does not require specialized, complicated equipment, unlike conventional techniques such as chemical vapor deposition (CVD), sputtering deposition, and atomic layer deposition (ALD) processes, which require vacuum sources and large footprint areas.[5]

Currently, many researchers are exploring the potential of low-temperature solution-processed inorganic devices. Although solution-based materials and processes can be applied widely in the fabrication of electronic devices, they still require the use of traditional photolithography processes to form the required pattern integration. Traditional photolithography processes require the use of chemicals such as photoresists (PR), developers, and removers, which can be toxic. These processes also have a number of demerits: they involve complicated steps and layer-by-layer processing, which have high associated costs; and the patterned films can degrade because of the chemical damage that takes place during the removal steps.[6] Although direct-printing methods such as inkjet printing, slit-die coating, screen-printing, gravure printing, and imprinting have been researched extensively, there are still problems such as the controllability of the shape, size, uniformity, and thickness of the films formed.[7] However, if photosensitive functionalized solutions were to be used to prepare films for device fabrication using solution processes, it might be possible to develop a very simple, environmentally friendly process for device fabrication because the photosensitive gel film itself would behave as the photoresist. Furthermore, irradiation with ultraviolet (UV) light could help to decompose the organic residuals on the films rapidly and enable phase transitions while accelerating the metal-oxide-metal (M-O-M) condensation and formation of high-purity oxide films.[8] In particular, the photosensitivity of the formed films can be controlled by combining several photosensitive additives with the starting material. Some approaches have independently investigated low-temperature processes, such as novel precursor synthesis, critical control of material composition,[2] UV annealing,[11] and postannealing process optimization.[12] However, approaches that result in the

Received: November 15, 2012
Accepted: March 28, 2013
Published: March 28, 2013

Scheme 1. Procedures Used for the UV-Irradiated Directly Photopatternable IGZO Solution and the Fabrication of IGZO TFTs

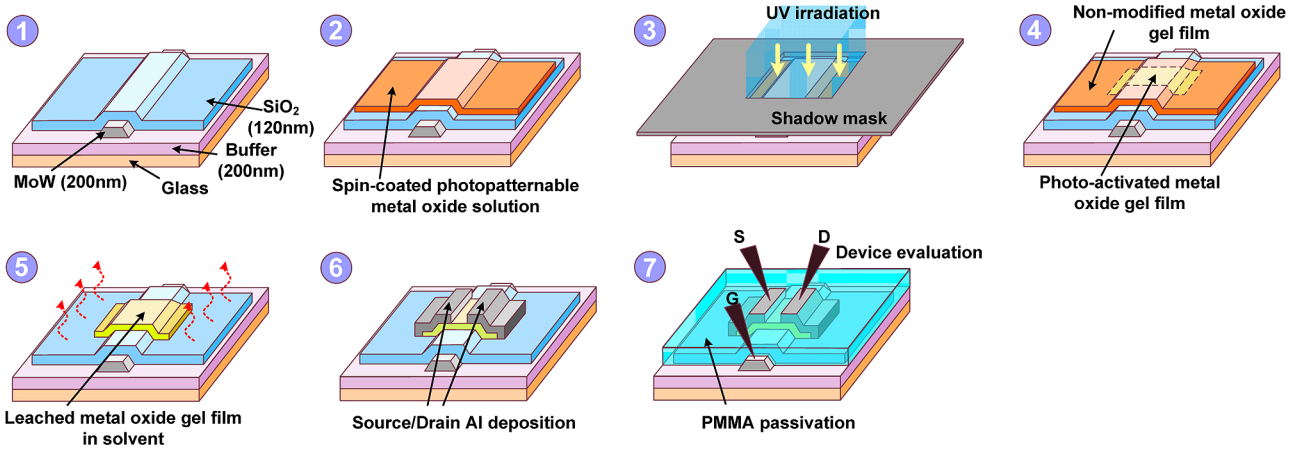

formation of direct patternable films at low temperatures while making use of photopyrolysis phenomenon have not worked for the fabrication of metal-oxide thin-film transistors (TFTs). Here, we report a simultaneously combustible and directly photopatternable solution-based approach on the oxide semiconductor films and their TFTs at low temperatures for the mass production of solution-processed metal-oxide-semiconductor devices. First, we fabricated high-reliability- direct-patterned InGaZnO (IGZO) TFTs using a chemically modified photoreactive metal-oxide solution. Then, we synthesized a combustible and photoreactive In_2O_3 solution, which was used to fabricate In_2O_3-based TFTs at 250 °C.

2. EXPERIMENTAL PROCEDURE

2.1. Solution Synthesis of Photoreactive IGZO and In_2O_3. A 0.3 M reference IGZO solution was prepared by dissolving 3.0 M indium nitrate hydrate ($In(NO_3)_3{\cdot}xH_2O$), 0.25 M gallium nitrate hydrate ($Ga(NO_3)_3{\cdot}xH_2O$), and 1.0 M zinc nitrate hydrate ($Zn(NO_3)_2{\cdot}xH_2O$) in 2-methoxyethanol (2ME). Then, 1.0 M monoethanolamine (MEA) (C_2H_7NO) and 1.5 M acetic acid (CH_3COOH) were added to stabilize the sol and make it transparent and homogeneous. After being stirred vigorously for 1 h at 60 °C, the IGZO solution was aged for 24 h. To synthesize an IGZO solution chemically modified by benzoylacetone, i.e., a BzAc-IGZO solution, benzoylacetone (BzAc) ($C_6H_5COCH_2COCH_3$) was mixed in the reference IGZO solution in the molar ratio: (In + Ga + Zn)/(BzAc) = 1. The solution was then stirred and aged for 24 h. To synthesize the In_2O_3 solution, weused indium nitrate hydrate as the starting material and was dissolved in 2ME to give a 0.3 M solution. Then, 1.5 M nitric acid (HNO_3) and acetylacetone (AcAc) were added to the In_2O_3 solution: these additives acted as an oxidizer and supported photoreactivity, respectively, while also acting as a fuel. The In_2O_3 solution containing HNO_3 and AcAc as additives (NAc-In_2O_3) was filtered through a membrane with 0.2 μm pores before being spin-coated.

2.2. Preparation of Patterning Process. In the direct photopatterning process used in this study, which is shown in Scheme 1, the BzAc-IGZO and NAc-In_2O_3 solutions were spin coated onto substrates and the coated substrates were soft-baked for 2 min at 90 °C. A flexible substrate was used for the NAc-In_2O_3 solution. The coated substrates were then irradiated using a high-pressure mercury UV lamp (Execure 4000-D, Hoya), while contacting the channel mask with a width of 2000 μm and length of 1000 μm (W x L) for 10 min in air. The main peaks of the UV lamp were at 253.7, 294.7, 302.2, and 365.0 nm (the power density of the radiation was 113 mW cm^{-2}; see Figure S4 in the Supporting Information). After lifting off the channel mask, the gel films were leached in ethanol (C_2H_6O) for 1 min. The non-UV irradiated regions of the films dissolved in the ethanol, whereas the insoluble irradiated regions remained.

2.3. Fabrication of IGZO and In_2O_3 TFTs. To fabricate IGZO-based TFTs, we used a bottom-gate and top-contact TFT structure. To fabricate the gate electrode, a 200-nm-thick molybdenum–tungsten (MoW) film was deposited on a glass substrate by radio frequency (RF) sputtering. A 120-nm-thick tetraethyl orthosilicate (TEOS) layer was deposited on the gate electrode using plasma-enhanced chemical vapor deposition (PECVD) to form the gate dielectric. The In_2O_3-based TFT was fabricated on a polyimide substrate; its structure was follows: SiO_x (thickness = 200 nm)/Mo (thickness = 200 nm)/SiO_x-SiN_x (thicknesses = 200 and 200 nm, respectively)/polyimide (PI) (thickness =20 μm). Spin-coated channel layers were applied at 3000 rpm for 30 s under N_2 using the IGZO and In_2O_3 solutions. After each non- or pattering process of IGZO films, they were annealed at 350 °C for 1 h in air. The patterned In_2O_3 film was annealed at 250 °C for 1 h in air. The Al source and drain (S/D) electrodes (thickness = 200 nm) were deposited by RF sputtering. The channel region was defined with a width of 1000 μm and length of 150 μm (W/L). Finally, a polymethyl methacrylate, (PMMA), passivation layer was spin-coated onto the channel layer at 1500 rpm over 30 s and annealed at 150 °C for 15 min. For comparison, we prepared nonpatterned and conventional PR-patterned IGZO TFTs. The electrical characteristics of the devices were measured in a dark box in ambient air using an Agilent 4156C precision semiconductor parameter analyzer.

Analysis of IGZO and In_2O_3 Films and TFTs. Positive and negative bias stress (PBS and NBS) tests with durations of 1,000 s were performed using V_{GS} ± 20 V at a fixed drain voltage (V_{DS}) of 10.1 V, whereas the transfer characteristics were measured at a fixed V_{DS} of 10.1 V to investigate variation in the performance of the TFTs under stress. The surface roughness of the films was analyzed using an atomic force microscopy (AFM) (XE-150, Park systems). Images of device patterns were taken using an optical microscopy (OM) (BX-51, Olympus) and a field emission scanning electron microscope (FE-SEM) (JSM-6701F, JEOL). Variation in the chemical compositions of the reference-IGZO and BzAc-IGZO films was observed using a Fourier transform infrared spectrometry (FT-IR) (Vertex 70, Bruker Optic). The optical absorption of the films was determined using an UV–visible (UV–vis) spectroscopy (Optizen 2120UV, MECASYS CO.). The actual thickness of the films after the final annealing of the IGZO channel layers was measured using a surface profilometer (Alpha Step 200, Tencor). Thermogravimetric analysis (TGA) and differential thermal analysis (DTA) of the solutions were performed using 20–30 mg solutions using a TGA analyzer (TA-Q600, TA Instruments) in ambient air. The heating rate during the analyses was fixed at 10 °C min^{-1}.

dx.doi.org/10.1021/am302722h | ACS Appl. Mater. Interfaces 2013, 5, 3565–3571

3. RESULTS AND DISCUSSION

3.1. Chemical Reactions of Photoreactive BzAc-IGZO Films. Figure 1a shows the Fourier transform-infrared (FT-IR)

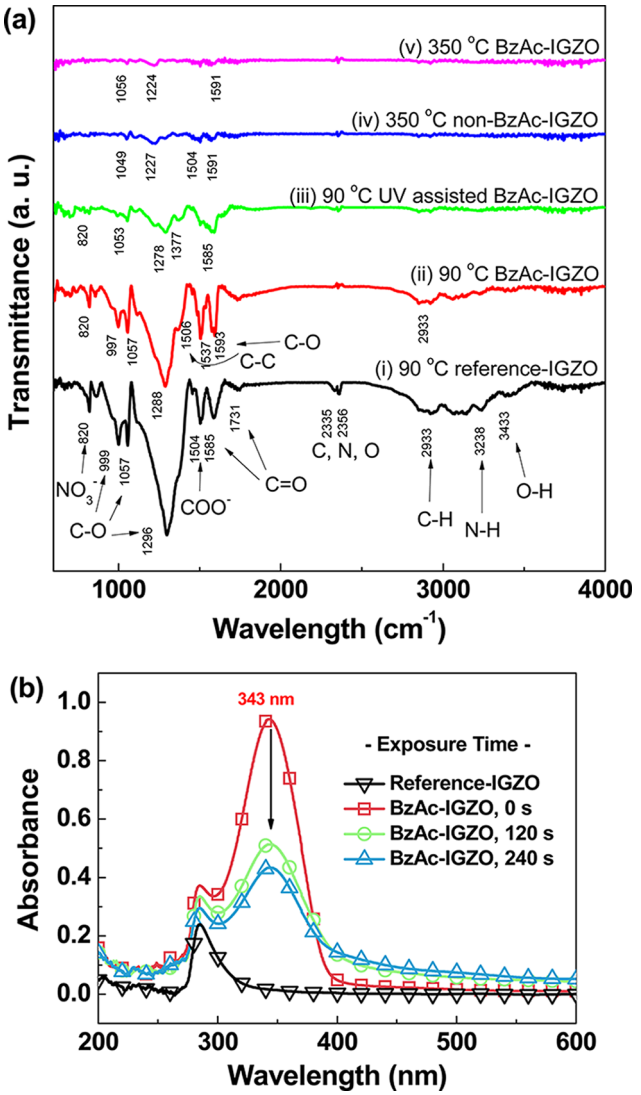

Figure 1. (a) FT-IR spectra of the reference-IGZO and BzAc-IGZO films as functions of the UV irradiation and annealing temperature and (b) the variation in the photoabsorption on the BzAc-IGZO solution with increasing UV irradiation time.

spectra of the reference-IGZO and BzAc-IGZO films as functions of the wavelengths of the UV radiation and annealing temperature. Curve (i) shows the spectrum of the reference-IGZO sample that was prebaked at 90 °C. The broad peaks at 3433, 3238, and 2933 cm^{-1} were related to the O−H stretching vibration, asymmetric N−H stretching vibrations of MEA, and symmetric and asymmetric CH_3 stretching vibrations, respectively.[13,14] The peaks at 1731, 1585, and 1504 cm^{-1} were assigned to the C−O stretching vibrations and COO^- asymmetric vibrations of carboxylic acid and acetic acid, respectively. The sharp peaks at 1296, 1057, and 999 cm^{-1} were attributable to the C−O stretching vibrations of the byproduct of the C−O−C bond.[14] The peak at 820 cm^{-1} was related to NO_3^- deformation.[15] Curve (ii) shows the spectrum of the BzAc-IGZO sample that was prebaked at 90 °C. peaks appeared at 1593 and 1506 cm^{-1} owing to the addition of BzAc. These peaks could be assigned to the C═O and C═C bonds formed by the chelation of BzAc with a metal cation.[16] This BzAc chelate bond with the IGZO precursor showed strong absorption at 343.8 nm as shown in Figure 1b. Furthermore, the intensity of the absorption peak of the BzAc-IGZO film decreased gradually with increasing UV-irradiation time, indicating that the $\pi-\pi^*$ transition occurred on UV irradiation and the chelate rings (BzAc-) were decomposed by the photoexcited electrons partially distributed over oxygen atoms. This absorption peak represented the photoreactivity of the BzAc-IGZO film, as shown in Figure 2 (detailed images are shown in Figure S9 in the Supporting Information).[17] The $\pi-\pi^*$ transition altered the solubility of the BzAc-IGZO film in specific chemical solvents such as 2ME, ethanol, and methanol. Curve (iii) shows the spectrum of the UV-irradiated BzAc-IGZO film. During the UV irradiation, the peaks of the carbon-containing organic groups, including those of the solvent, precursor ligands, and stabilizers, decreased rapidly in intensity. The rapid organic volatilization and decomposition of the BzAc-IGZO film can be explained by the ligand-to-metal charge transfer, which was due to the photoexcited thermally unstable molecules and their dissociation into metal-containing ligands.[18,19] Furthermore, UV irradiation supports the formation of a high-purity oxide film at low temperatures, regardless of the addition of BzAc. These results are consistent with the photoreaction in the formation of metal oxide films at low-temperatures. As a result, we obviously found that the photopatterning phenomena of the BzAc-IGZO film occurred because of the broad absorbance peak (300 to 380 nm) as shown in Figure 1b and that the long-wavelength bands of 302.2 and 365.0 nm could support the patterning process. In the case of the short-wavelength bands of 253.7 and 294.7 nm, these could effectively decompose the organic ligands in metal oxide precursors and promote the oxidation of the IGZO film owing to the photochemical reactions and the generated ozone radicals.[1,10] Curves (iv) and (v) show the spectra of the reference-IGZO and UV-irradiated BzAc-IGZO films annealed at 350 °C, respectively. The spectra of as-annealed BzAc-IGZO films did not show the peaks

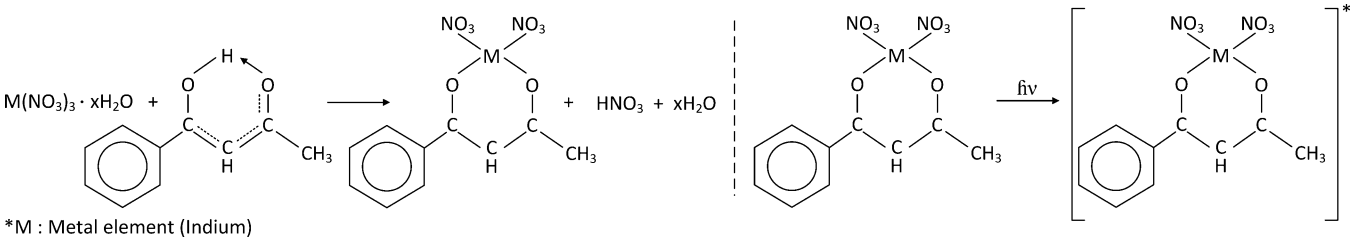

Figure 2. Reaction mechanism for the photolysis of the gel film of IGZO chemically modified with BzAc.

associated with organic compounds, despite the addition of BzAc. That is, the addition of BzAc did not affect the chemical composition or residual organics of the finalized oxide film that had been irradiated with UV light and annealed at a relatively low temperature (350 °C).

3.2. Analysis on the Device Performance of Directly Photopatterned IGZO TFTs. Figure 3 shows the transfer characteristics and images of the patterns (inset) of the various IGZO TFTs fabricated using different patterning methods (detailed images are shown in Figure S6 in the Supporting Information). As shown in Figure 3a, the reference IGZO TFTs without the pattern process showed a very large gate-source leakage current (IGS). This was attributed to the leakage current occurring at the overlap of the wide contact area between the S/D and gate electrodes in the nonpatterned area. In addition, this gate leakage current is responsible for the increase in the electric power consumption when contact resistance occurs between the S/D and gate electrodes (RGD and RGS).[20,21] In comparison, the directly photopatterned IGZO TFTs showed very low leakage currents, which were less than 20 pA. However, the hysteresis in the case of the PR-patterned IGZO TFTs was much larger than that seen for the nonpatterned and directly photopatterned IGZO TFTs. Typically, a degraded back channel increases the trap states that originate from chemical species or water molecules, and hysteresis would depend on the degree of the back channel damage. The PR stripping process degraded the back surface of the IGZO film, and the defects in the IGZO film resulted in a change in the carrier concentration.[9] The altered carrier concentration of the back channel region affected the overall electrical properties of the IGZO film and degraded the TFT behavior. The surface roughness of the nonpatterned, PR-patterned, and directly photopatterned IGZO films was 0.186, 1.818, and 0.443 nm, respectively (see Figure S1 in the Supporting Information). These results are consistent with the changes in the back surfaces of the IGZO films resulting from the PR stripping process.

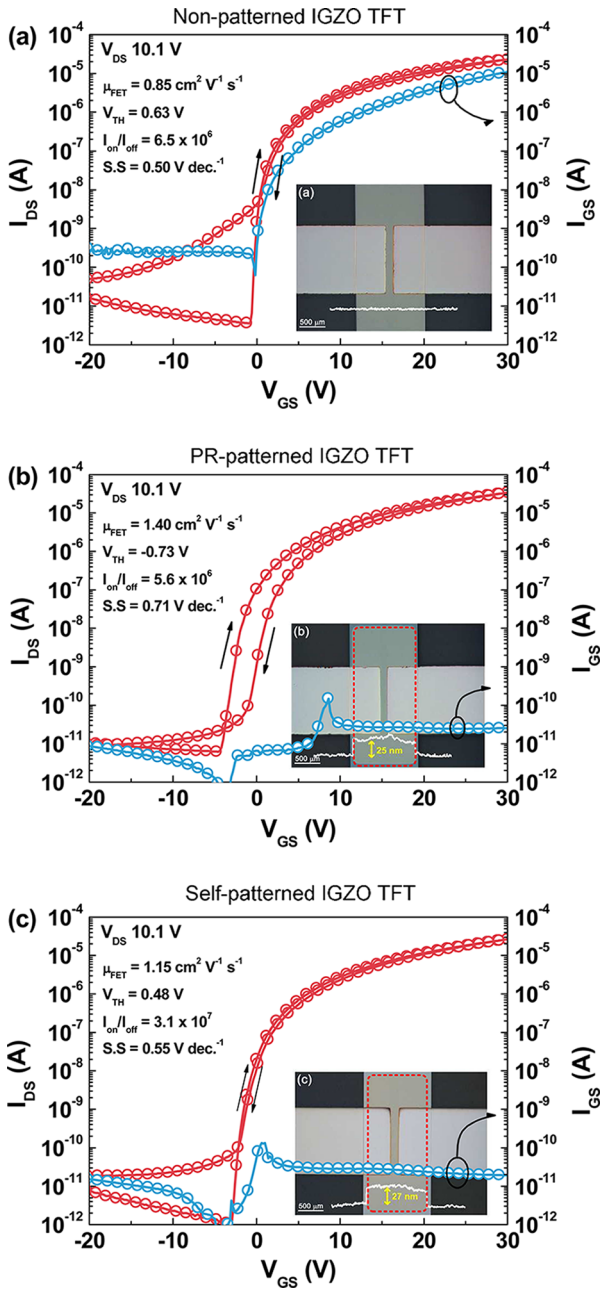

Figure 3. Transfer characteristics of the (a) nonpatterned, (b) PR-patterned, and (c) directly photopatterned IGZO TFTs. The insets show the shapes patterned using different isolation processes.

Figure 4 shows the output characteristics (I_{DS}–V_{DS}) of the (a) nonpatterned and (b) directly photopatterned IGZO TFTs. A high leakage current was clearly observed in the case of the nonpatterned IGZO TFT, even at $V_{GS} \approx 0$ V. In comparison, the leakage current in the case of the directly photopatterned TFT was effectively suppressed. This result is consistent with the formation of pathways for the leakage current described above. As a result, the directly photopatterned IGZO film acted as an excellent channel layer, regardless of the addition of BzAc, and clearly exhibited better device characteristics than those of the nonpatterned IGZO TFT.

Figure 5 shows the variation in the threshold voltage (ΔV_{TH}) of the differently patterned IGZO TFTs during (a) positive bias stress (PBS) and (b) negative bias stress (NBS) tests. The value of ΔV_{TH} for the directly photopatterned IGZO TFT, i.e., ΔV_{TH} = 3.06 V, was much lower than that of the PR-patterned IGZO TFT (7.24 V) during the PBS test. In addition, the V_{TH} shift for the directly photopatterned IGZO TFT of (negative) 2.47 V was the lowest measured during the NBS tests. Notably, although the surface roughness of the nonpatterned IGZO film was the smallest, the directly photopatterned IGZO TFT exhibited the highest stability during the bias stress tests. Typically, the performance of an IGZO TFT depends on various factors such as the morphology of the interface between the channel and the gate insulator, the defects in the channel bulk, and the presence of organic impurities.[22] Accordingly, these results could be attributed to the high quality of the bulk and the interface of the directly photopatterned IGZO film formed, which was because of the rapid volatilization of the IGZO gel film and the M-O-M condensation it experienced during the initial UV irradiation, as shown by its FT-IR spectra.

3.3. Combustion Processing of the Directly Photopatterned In_2O_3 TFT. To confirm the formation a simultaneously directly photopatterned, low-temperature metal-oxide semiconductor, we fabricated a device at the low temperature of 250 °C using a directly photopatterned In_2O_3 film coated on a polymer substrate, as shown in Figure 6e. As described in the Experimental section, we used a novel chemical route to form the directly photopatterned oxide semiconductor,

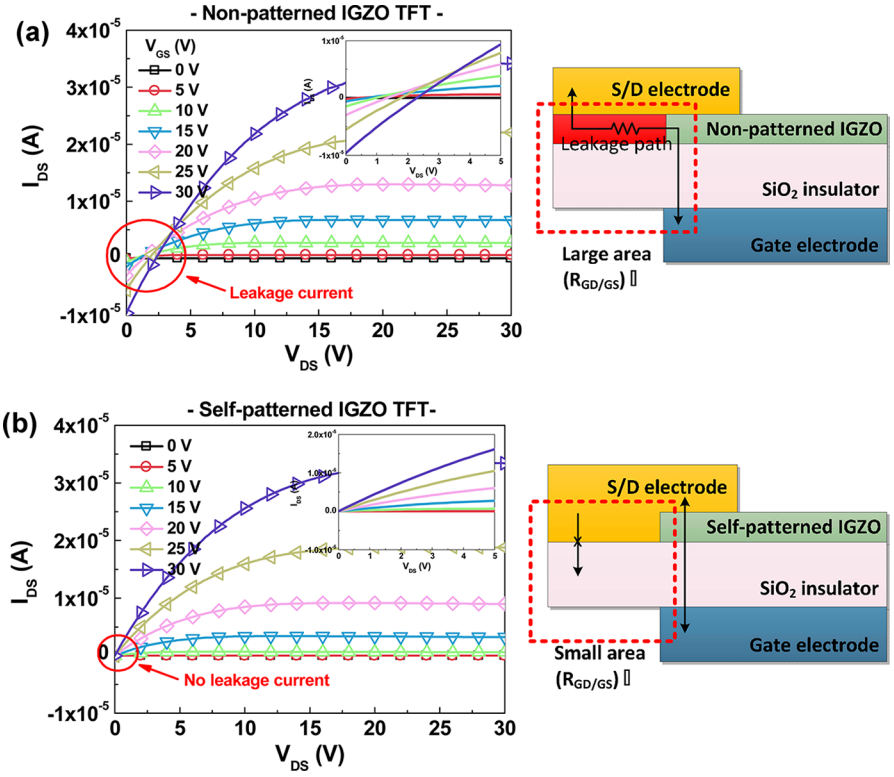

Figure 4. (Left) I_{DS}–V_{DS} curves and (right) leakage current pathway schematics of the (a) nonpatterned and (b) directly photopatterned IGZO TFTs. The pathways formed because of the contact resistance between the S/D electrodes and channel region.

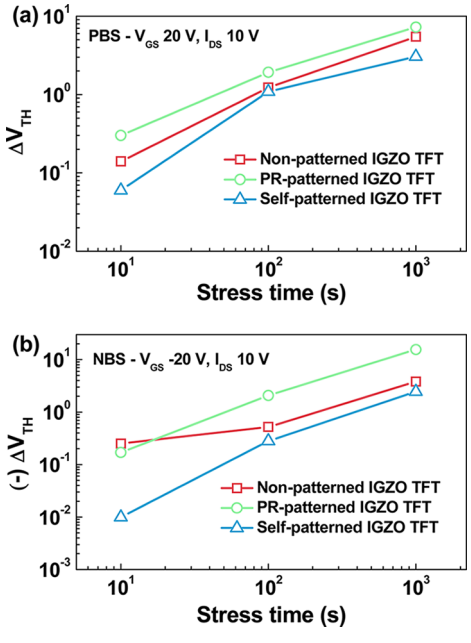

Figure 5. ΔV_{TH} of the nonpatterned, PR-patterned, and directly photopatterned IGZO TFTs under (a) PBS and (b) NBS tests.

using the additives nitric acid (HNO_3) and acetylacetone (AcAc). As mentioned earlier, one route for the low-temperature formation of a solution-processed metal oxide is the combustion method, which makes use of an oxidizer and a fuel.[2] Although the combustion method results in the formation of a metal oxide at temperatures lower than 250 °C, it still requires the use of photolithography to form the appropriate patterns of the channel layers. However, our novel method using the In_2O_3 solution containing HNO_3 as an oxidizer and AcAc (NAc-In_2O_3) as a fuel and a photoreactive additive resulted in the formation of directly photopatterned layers as shown in Figure 6a. The HNO_3 oxidizer promotes self-energy generation and densification of the films via the weak bonding of NO_3^- and low-condensation rate.[12] As a fuel additive, AcAc causes a very strong exothermic reaction in the In_2O_3 solution.[2] This chemical reaction of the combined solution, which was highly exothermic, resulted in the rapid decomposition of organic compounds at low temperatures, as shown in Figure 6b (comparison with conventional In_2O_3 solution is shown in Figure S5b in the Supporting Information). Surprisingly, we observed another distinct effect of the UV absorption on the NAc-In_2O_3 solution as shown in Figure 6a. In the absorption spectrum of the NAc-In_2O_3 solution, a new broad absorption band was observed at wavelengths of 250–400 nm; this change in the absorption spectrum was attributed to the π–π^* transition in the chelate ring of AcAc as shown in Figure S11. Furthermore, the UV-irradiated NAc-In_2O_3 film decomposed rapidly, as did the BzAc-IGZO film. Ultimately, In_2O_3, which was made combustible by the addition of HNO_3 and AcAc, could be functionalized for the directly photopatterning process at low temperatures. As mentioned above, the ultimate goal of the solution-based process is not only to form functional directly photopatterned films but also to enable the fabrication of oxide-based TFTs on flexible substrates at low temperatures. To demonstrate this combined approach to the fabrication of flexible devices, we formed the combustible, directly photopatternable NAc-In_2O_3 precursor solution on a flexible polyimide substrate. The resulting In_2O_3-based TFT (whose detailed structure is as shown in the Experimental section) on the flexible polyimide substrate performed well, with a field-

dx.doi.org/10.1021/am302722h | ACS Appl. Mater. Interfaces 2013, 5, 3565–3571

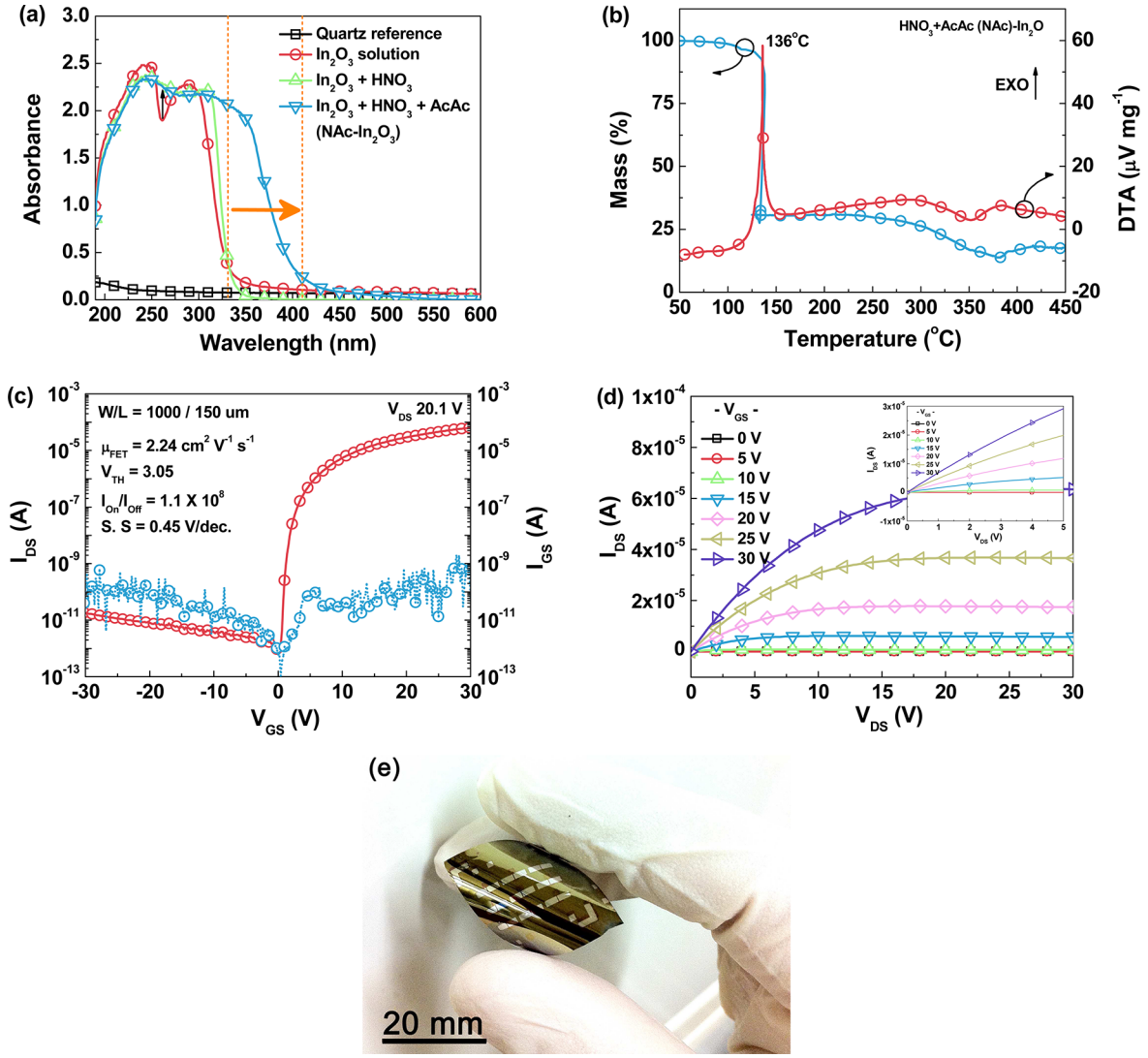

Figure 6. (a) UV−vis absorbance peaks of In_2O_3 solutions with different additives, such as no additives, HNO_3, and HNO_3 + AcAc. (b) Results of the TGA and DTA of the NAc-In_2O_3 solution. (c) I_{DS}−V_{GS} transfer, (d) I_{DS}−V_{DS} output, and (e) optical image of an In_2O_3 TFT fabricated on a flexible substrate.

effect mobility of 2.24 $cm^2\ V^{-1}\ s^{-1}$, subthreshold voltage swing of 0.45 V/dec., and I_{on}/I_{off} ratio of 1×10^8.

4. CONCLUSION

In this work, we have demonstrated the fabrication of directly photopatternable metal-oxide-semiconductor-based thin-film transistors. The UV-irradiated BzAc-IGZO solution showed the π−π^* transition, and its chelate rings could be decomposed by the photoexcited electrons surrounding oxygen atoms. This showed that it was possible to form directly photopatterned oxide films owing to the solubility of the IGZO gel film in ethanol. The readily and rapidly formed directly photopatterned IGZO film was very pure, with a very smooth surface, and the resulting directly photopatterned IGZO TFT had excellent electrical performance. This was attributed to the rapid decomposition of the organic compounds in the IGZO gel film because of its initial pyrolysis when irradiated with UV light. In addition, we have demonstrated for the first time, to the best of our knowledge, a combustible, directly photopatternable In_2O_3-based TFT was fabricated successfully on a flexible polyimide substrate at 250 °C. As a result, this work establishes the generalizability of the solution-based synthesis process for the formation of directly photopatternable films at low temperatures. This process should be useful in the high-throughput fabrication of solution-processed, oxide-based TFTs via a PR-free process.

■ ASSOCIATED CONTENT

Supporting Information

Optical microscope, SEM and AFM images of different pattern processed IGZO films, spectral distribution of the high-pressure mercury UV lamp, TGA and DTA spectra of In_2O_3 solutions with different additives, the parameter of chemical reaction in FT-IR, and photoreaction process in BzAc and AcAc chelated metal oxide solutions. This material is available free of charge via the Internet at http://pubs.acs.org.

■ AUTHOR INFORMATION

Corresponding Author

*E-mail: hjk3@yonsei.ac.kr.

Notes

The authors declare no competing financial interest.

■ ACKNOWLEDGMENTS

This work was supported by the National Research Foundation of Korea (NRF) grant funded by the Korean Ministry of Education, Science and Technology (MEST) [no. 2011-0028819].

■ REFERENCES

(1) Kim, Y.-H.; Heo, J.-S.; Kim, T.-H.; Park, S.; Yoon, M.-H.; Kim, J.; Oh, M. S.; Yi, G.-R.; Noh, Y.-Y.; Park, S. K. *Nature* **2012**, *489*, 128−132.
(2) Kim, M.-G.; Kanatzidis, M. G.; Facchetti, A.; Marks, T. J. *Nat. Mater.* **2011**, *17*, 382−388.
(3) Banger, K. K.; Yamashita, Y.; Mori, K.; Peterson, R. L.; Leedham, T.; Rickard, J.; Sirringhaus, H. *Nat. Mater.* **2010**, *10*, 45−50.
(4) Walker, D. E; Major, M.; Yadzi, M. B.; Klyszcz, A.; Haeming, M.; Bonrad, K.; Melzer, C.; Donner, W.; Seggern, H. V. *ACS Appl. Mater. Interfaces* **2012**, *4*, 6835−6841.
(5) Pasquarelli, R. M.; Ginley, D. S.; O'Hayre, R. *Chem. Soc. Rev.* **2011**, *40*, 5406−5441.
(6) Han, H.; Bissell, J.; Yaghmaie, F.; Davis, C. E. *Langmuir* **2010**, *26*, 515−520.
(7) Parashkov, R.; Becker, E.; Riedl, T.; Johannes, H.; Kowalsky, W. *Proc. IEEE* **2005**, *93*, 1321−1329.
(8) Han, Y.-H.; Taylor, A.; Mantle, M. D.; Knowles, K. M. *J. Sol−Gel Sci. Technol.* **2007**, *43*, 111−123.
(9) Ryu, S. H.; Park, Y. C.; Mativenga, M.; Kang, D. H.; Jang, J. *ECS Solid−State Lett.* **2012**, *1*, Q17−Q19.
(10) Han, S.-Y.; Herman, G. S.; Chang, C.-H. *J. Am. Chem. Soc.* **2011**, *133*, 5166−5169.
(11) Shinmou, K.; Tohge, N.; Minami, T. Jpn. *J. Appl. Phys.* **1994**, *33*, 1181−1184.
(12) Jiang, K.; Anderson, J. T.; Hoshino, K.; Li, D.; Wager, J. F.; Keszler, D. A. *Chem. Mater.* **2011**, *23*, 945−952.
(13) Kim, G. H.; Shin, H. S.; Ahn, B. D.; Kim, K. H.; Park, W. J.; Kim, H. J. *J. Electrochem. Soc.* **2009**, *156*, H7−H9.
(14) Socrates, G. *Infrared Characteristic Group Frequencies*; John Wiley & Sons: New York, 1994.
(15) Song, K.; Jung, Y.; Kim, Y.; Kim, A.; Hwang, J. K.; Sung, M. M.; Moon, J. *J. Mater. Chem.* **2011**, *21*, 14646−14654.
(16) Liang, C. Y.; Schimitschek, E. J.; Trias, J. A. J. *Inorg. Nucl. Chem.* **1970**, *32*, 811−831.
(17) Weihua, Z.; Gaoyang, Z.; Zhiming, C. *Mater. Sci. Eng., B* **2003**, *99*, 168−172.
(18) Habouti, S.; Solterbeck, C.-H.; Es-Souni, M. *J. Sol−Gel Sci. Technol.* **2007**, *42*, 257−263.
(19) Calzada, M. L.; González, A.; Poyato, R.; Pardo, L. *J. Mater. Chem.* **2003**, *13*, 1451−1457.
(20) Hong, D.; Yerubandi, G.; Chiang, H. Q.; Spiegelberg, M. C.; Wager, J. F. *Crit. Rev. Solid-State Mater.* **2008**, *33*, 101−132.
(21) Wager, J. F.; Keszler, D. A.; Presley, R. E *Transparent Electronics*; Springer: New York, 2008; p 136.
(22) Rim, Y. S.; Jeong, W. H.; Kim, D. L.; Lim, H. S.; Kim, K. M.; Kim, H. J. *J. Mater. Chem.* **2012**, *22*, 12491−12497.